Proceedings of IMECE'03
2003 ASME International Mechanical Engineering Congress
Washington, D.C., November 15–21, 2003

IMECE2003-42079

FORCE CONTROL OF LINEAR MOTOR STAGES FOR MICROASSEMBLY

Jason J. Gorman and Nicholas G. Dagalakis
Intelligent Systems Division
National Institute of Standards and Technology
Gaithersburg, Maryland 20899-8230
gorman@cme.nist.gov

ABSTRACT

The microassembly of microelectromechanical systems from various micro-components requires the development of many new robotic capabilities. One of these capabilities is force control for handling micro-scale components with force control resolution on the order of micronewtons. In this paper, the force control of linear motor stages is discussed with application to the microassembly of MEMS. Linear motor stages provide an attractive solution for microassembly robots because they have a large working volume and can achieve high-precision positioning. However, the nonlinear friction and force ripple effects inherent in linear stages provide an obstacle to the required level of force control. A model of a single motor stage has been developed including dynamic friction effects. Based on this model, a robust nonlinear force controller has been designed to meet the microassembly requirements. The controller has been tested in simulation to demonstrate its effectiveness.

Keywords: microassembly, force control, linear motor, sliding mode control

INTRODUCTION

The development of manufacturing processes, as well as applications, for microelectromechanical systems (MEMS) has grown steadily over the last decade. Although silicon micromachining has led the way in terms of manufacturing of MEMS, it also has many limitations which hinder the progress of possible applications. These limitations include the material selection, structure aspect ratio and the inability to make true three dimensional structures. In some cases, these limitations have been overcome by modifications to the silicon micromachining process, or the use of advanced processes such as deep reactive ion etching. However, in general, these limitations continue to shape the MEMS design procedure, the breadth of applications and the available markets.

Many researchers have investigated other micromanufacturing techniques which could overcome these disadvantages. Some of these include LIGA, micro-molding, micro-stereo lithography, micro-electro-discharge machining, and laser micromachining [1]. By utilizing several of these processes in tandem, it is possible to create 3-D structures with virtually unlimited geometry and aspect ratio. However, their main drawback is that microelectronics can not be manufactured using these techniques. Therefore, an integrated MEMS device can not be manufactured using a single process plan, as in silicon micromachining. This limitation is possibly the largest single motivator for the development of microassembly technologies.

The use of microassembly would allow micro-components to be manufactured using a number of different processes and then integrated into a MEMS device by mechanical manipulation. Microassembly has been investigated by several researchers with varying goals. Surveys and overviews of this research have been presented in [2-4]. The tools required for microassembly are similar to that of macro-scale assembly: A robotic mechanism with the necessary degrees of freedom; accurate sensing of position and contact force; models of mechanisms and contacts; and algorithms for motion and force control. However, due to the scaling issues involved in microassembly, the approaches to developing these tools are often drastically different as compared to the macro scale.

In this paper, a microassembly robot composed solely of linear motor stages and a direct drive rotational stage is proposed. This approach is often not considered viable for micro-scale positioning and manipulation due to friction and ripple force effects. However, recently there has been some impressive research presented on micropositioning using linear motor stages. Xu and Yao [5] and Tan et al. [6] have achieved high-speed tracking with tracking errors on the order of several micrometers. Sub-micrometer positioning has also been demonstrated for specific motion plans by Wu and Perng [7]. Furthermore, sub-micrometer tracking has been shown for ball-

screw motion stages by Ro et al. [8], which typically have larger friction forces than linear motor stages. Although there has been significant research on micropositioning using linear motor stages, there has been little on their operation in force control with micronewton resolution.

Most of the research on force control for micromanipulation has been limited to piezoelectric actuated mechanisms. This includes the work by Nelson et al. [9], which demonstrates force regulation on the order of nanonewtons, as well as the dual-probe micromanipulator presented by Tanikawa et al. [10]. The research presented in this paper is concentrated on the development of a force control approach for linear motor stages with force regulation on the order of micronewtons.

The proposed control approach is based on a detailed dynamic model of a single linear motor stage. This model includes a representation of the friction forces and ripple force, which dominate the stage's motion. The friction is modeled using a dynamic approach based on the work of Canudas de Wit et al. [11]. The complexities of this model are demonstrated by open loop simulations.

Based on this model, a force controller has been developed. First, a robust motion controller will be discussed, which will be used as the inner motion loop of the force control design. The motion controller is designed using sliding modes and a friction observer which is used to estimate the friction force for direct cancellation. The force control law is then presented, which is based on the standard proportional-integral approach. Finally, simulation results are presented for the dynamic model and proposed control design which demonstrate the force regulation performance and the robustness properties to uncertain friction and force ripple parameters. Before addressing the modeling and control issues, a discussion on the workspace and performance requirements for the microassembly of MEMS, which motivates the use of linear motor stages, will be presented.

MICROASSEMBLY REQUIREMENTS

The requirements for a microassembly robot have not been well defined in the literature, largely due to varying opinions on the role of microassembly and the many applications which it can address. In this paper, it is assumed that the role of the microassembly robot is to assemble MEMS devices from multiple micro-parts which can have critical dimensions from 2 μm to 500 μm. The parts may be connected to a process wafer or stored in bins. Each device will be assembled onto another process wafer.

Therefore, the workspace of the robot must be large enough such that the robot can reach each of the assembly points on the wafer and have access to the assembly parts on separate wafers or in part bins. The most common size wafer used in the processing of MEMS for silicon micromachining and other micromanufacturing processes is 75 mm in diameter. Therefore, a workspace with 100 mm of reach in both the *x* and *y* directions would be satisfactory. The required clearance in the *z* direction would be minimal, so 30 mm is chosen because it would allow a large range of end-effector tools to be used with the robot.

The performance requirements for microassembly of MEMS are based on the production costs of assembly and the

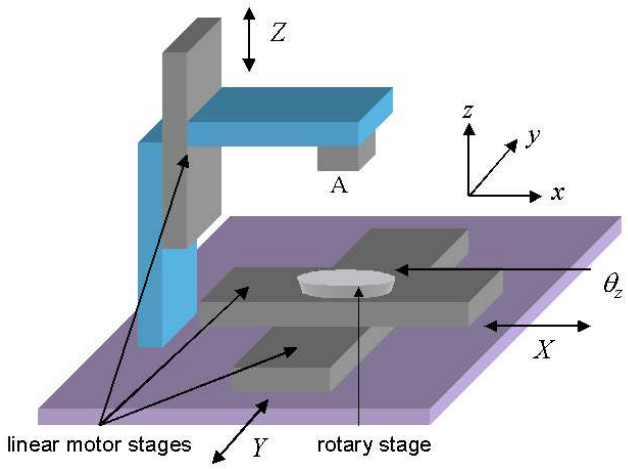

Fig. 1 Proposed microassembly robot design

tolerances for micro-part manufacturing. Although several different approaches for parallel microassembly have been discussed (see [2]), serial microassembly, or assembling a single device part by part, is the most straightforward. Furthermore, the development of serial assembly strategies will most likely lead to the development of parallel assembly innovations. In serial assembly, the assembly speed will drastically affect the cost of the device, similar to microelectronics board assembly. Therefore, a fast positioning system will be required, although it is difficult to quantify the bandwidth. Most micromanufacturing tolerances are dependent on lithography processes. In general, the accepted accuracy of a wafer stepper is around 1 μm for MEMS production (see [1]). Therefore, a positioning resolution and accuracy in the sub-micrometer range would also be required.

Most of the proposed robotic systems for microassembly in the literature do not meet these criteria for workspace, bandwidth and accuracy. Many of these mechanisms have limited workspaces, on the order of a few millimeters or less, such as those studied in [10], [12] and [13]. Others have used a dual-stage approach to meet the workspace and positioning requirements. Typically, a macro motion system and micro motion system are coupled, such as motor driven ball-screw linear stages and piezoelectric micropositioners [14,15]. Although both workspace and positioning requirements can be met using this approach, the bandwidth is usually low. Furthermore, the dual-stage system requires extensive hardware, complex algorithms and advanced metrology approaches, in order to compensate for the cross-talk errors between the micro and macro motions.

A more obvious and straightforward approach would be to use linear motor stages and direct drive rotational stages, such as the robot shown in Fig. 1. This approach would provide high assembly bandwidth and a large workspace. Similar designs have been considered by other researchers, such as Dechev et al. [16]. However, details of the modeling and control of such a robot for microassembly have not been presented in the literature.

The remainder of this paper will concentrate on the dynamic modeling and force control design for a single linear motor stage. These results have been used to develop detailed

numerical simulations of the stage during force regulation. This data will be used to design a microassembly robot such as the one described in Fig. 1. The dynamic model of the linear motor stage is presented in the following section.

DYNAMIC MODELING

There have been several approaches presented in the literature to modeling linear motor stages for high-precision motion control applications [5-7]. The dominant forces are due to friction effects, such as Coulomb friction, viscous friction and stiction, and force ripple. In most cases the electrical dynamics are ignored since they are at a much higher bandwidth than the mechanical dynamics and they are inherently stable. Therefore, the main modeling decisions are based on the required accuracy of the representation of the friction and force ripple effects.

Wu and Perng [7] have developed a hybrid friction model, which models the stiction effects in the presliding regime and the Coulomb and viscous forces in the sliding regime, separately. This is motivated by their goal to achieve nanometer scale positioning accuracy, which is heavily affected by the presliding forces. A static model of friction which includes Coulomb and viscous friction as well as the Stribeck effect, which represents the force peaking occurring at the transition between the presliding and sliding regimes, was presented by Xu and Yao [5]. Tan et al. [6] utilized a similar approach but added a sinusoidal model of the force ripple. The main drawback of the static friction model presented in [5] and [6] is that it does not include the forces in the presliding regime, which are critical to micropositioning and high-precision tracking at velocity reversals.

In this paper, a dynamic friction model developed by Canudas de Wit et al. [11] is used. This model incorporates the presliding and sliding friction regimes into a single dynamic equation, resulting in a straightforward implementation compared to the hybrid model discussed in [7]. In addition, the force ripple used by Tan et al. [6] will be included. The dynamic model will be derived in the following section. Simulations results of the open loop motion of the system will then be presented and discussed. This will be followed by a simple model of the contact force between a linear motor stage and process wafer during a microassembly operation.

Linear Motor Stage Model

When neglecting the electrical dynamics of the linear motor, the dynamics of a single stage can be written as follows:

$$m\ddot{x} + f_f + f_r + f_c = K_f u \tag{1}$$

where x is the displacement of the stage, m is the mass of the stage, f_f is the friction force, f_r is the force ripple, f_c is the external contact force during microassembly, K_f is the force constant of the motor, and u is the control input, which in this case is the motor current. The motor current is used in this particular case so that the motor dynamics can easily be added to the mechanical dynamics if found necessary. This model is similar to that shown in [5] and [6], except for the approach which will be used to represent the friction force, f_f. The equation of motion represented by Eq. (1) can be put into state-space form by assuming that $x_1 = x$ and $x_2 = \dot{x}$. This results in the following:

$$\dot{x}_1 = x_2 \tag{2}$$

$$\dot{x}_2 = -\frac{1}{m}\left(f_f + f_r + f_c\right) + \frac{K_f}{m}u \tag{3}$$

The friction force, f_f, can be modeled using the dynamic approach presented by Canudas de Wit et al. [11]. This approach is based on the concept that the contact between two moving planes can be modeled as a group of intertwined bristles. It is assumed that these bristles deform for small relative motions, but still maintain contact with other bristles, acting as springs between the two planes. When the bristles deform past a certain point, due to larger relative motion, they can no longer maintain contact and the two planes slide past each other. This effectively represents the presliding and sliding regimes of friction. The average deflection of the bristles is represented by the following dynamic equation:

$$\dot{z} = x_2 - \frac{|x_2|}{g(x_2)}z \tag{4}$$

where:

$$g(x_2) = \frac{1}{\sigma_0}\left(F_c + \left(F_s + F_c\right)e^{-\left(x_2/x_{2s}\right)^2}\right) \tag{5}$$

The friction force can then be written as:

$$f_f = \sigma_0 z + \sigma_1 \dot{z} + \sigma_2 x_2 \tag{6}$$

The parameters in Eqs. (4) and (5) must be determined experimentally. In particular, F_s is the peak friction force caused by the Stribeck effect, F_c is the Coulomb friction magnitude, σ_0 is the stiffness constant of the system in the presliding regime, σ_1 is the micro-damping constant, σ_2 is the viscous friction constant, and x_{2s} determines the decay of the Stribeck effect for increasing velocity.

When the system is in the sliding regime, the steady-state friction force can be written as:

$$f_{fss} = \left(F_c + \left(F_s + F_c\right)e^{-\left(x_2/x_{2s}\right)^2}\right)\frac{x_2}{|x_2|} + \sigma_2 x_2 \tag{7}$$

Therefore, the maximum friction force is bounded by the Stribeck effect force and viscous damping. This fact will be used later in the controller design.

The model for the force ripple, based on the work of Tan et al. [6], can be represented as:

$$f_r = A_{r1}\sin\omega x_1 + A_{r2}\cos\omega x_1 \tag{8}$$

where A_{r1} and A_{r2} are the force amplitudes of the force ripple and ω represents the spatial frequency of the motor core. Therefore, the force ripple acts as either a repulsive or attractive force depending on the position of the linear motor stage.

The dynamic model defined by Eqs. (2-8) has been tested in simulation to provide further understanding of this problem. The model parameters used for the simulations, which are based on the results in the above mentioned references, are σ_0 = 1 x 10^5 N/m, σ_1 = 316.2 N·s/m, σ_2 = 0.8 N·s/m, F_c = 1.2 N, F_s = 1.6 N, x_{2s} = 0.001 m/s, m = 2 kg, K_f = 10.4 N/A, ω = 314 rad/m, A_{r1} = 0.494 N, and A_{r2} = 0.078 N. In the first test, a sinusoidal current signal with a frequency of 1 Hz and a resulting force magnitude of 1 N was applied to the model. Since the amplitude is below the Stribeck effect constant, the system is expected to remain in the presliding regime. Fig. 2 shows the results of this test when the force ripple was neglected and Fig. 3 shows the results when the force ripple is included. It is clear that the presliding regime, or micro-dynamics as referred to in [7], is characterized by a nonlinear stiffness and a strong hysteresis in the force-displacement relationship. However, the addition of the force ripple in the model causes a drift in the hysteresis loop resulting from cogging. These nonlinearites can have a drastic effect on the micropositioning capabilities and must be compensated in the control design.

Fig. 4 shows the results of a second test, where the amplitude of the sinusoidal signal was set to 1.7 N, such that the initial stiction is overcome. This results in a stick-slip behavior, which is indicated by the flat portion of the position results and the nearly square force-displacement hysteresis loops. The control of this complex dynamic system will be discussed shortly. First, a simple model of the contact force during microassembly will be described.

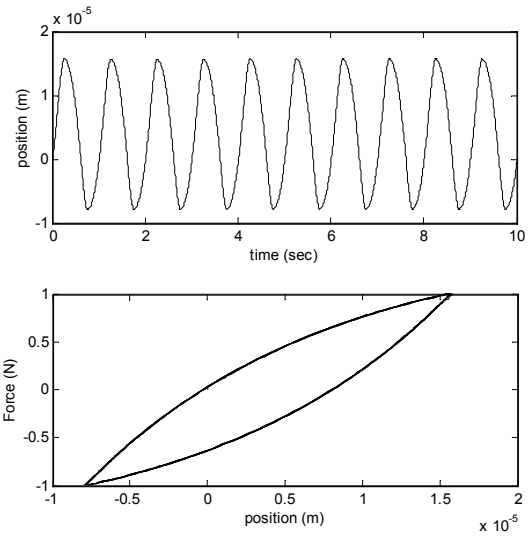

Fig. 2 Micro-dynamics without force ripple

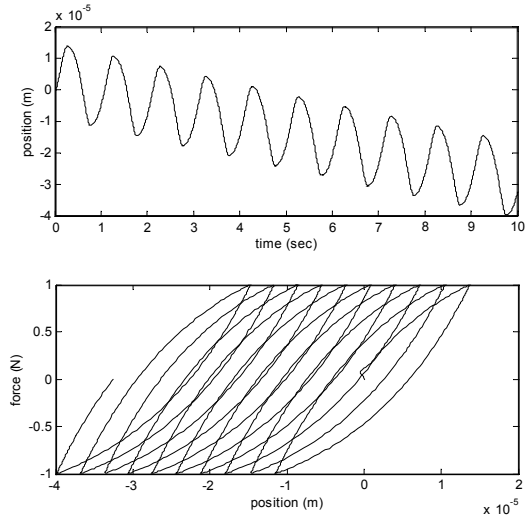

Fig. 3 Micro-dynamics with force ripple

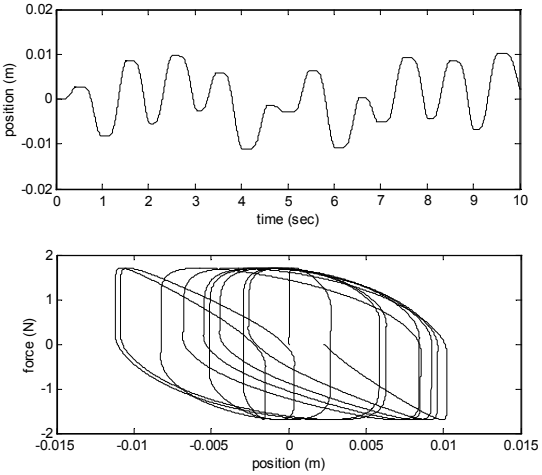

Fig. 4 Dynamics in sliding regime

Contact Force Model

A contact force model between the linear motor stage and the surface with which it interacts is needed for the testing of the proposed control approach in simulation. A possible microassembly scenario is depicted in Fig. 5a. The linear motor stage is used to move a microgripper holding a micro-part into contact with an assembly surface. The contact force is measured by a force sensor with resolution on the order of micronewtons. Due to the relative motion between the linear motor stage and process wafer, a force develops based on the stiffnesses of the microgripper, micro-part and wafer. Fig. 5b shows the simple spring model which can be expressed in equation form as:

$$f_c = \begin{cases} 0 & for \quad x_1 < x_i \\ \left(\dfrac{k_e\, k_s}{k_e + k_s} \right)(x_1 - x_i) & for \quad x_1 \geq x_i \end{cases} \qquad (9)$$

where x_i is the initial distance between the linear motor stage and wafer, k_e is the stiffness of the microgripper and micro-part, and k_s is the stiffness of the wafer surface. The values of

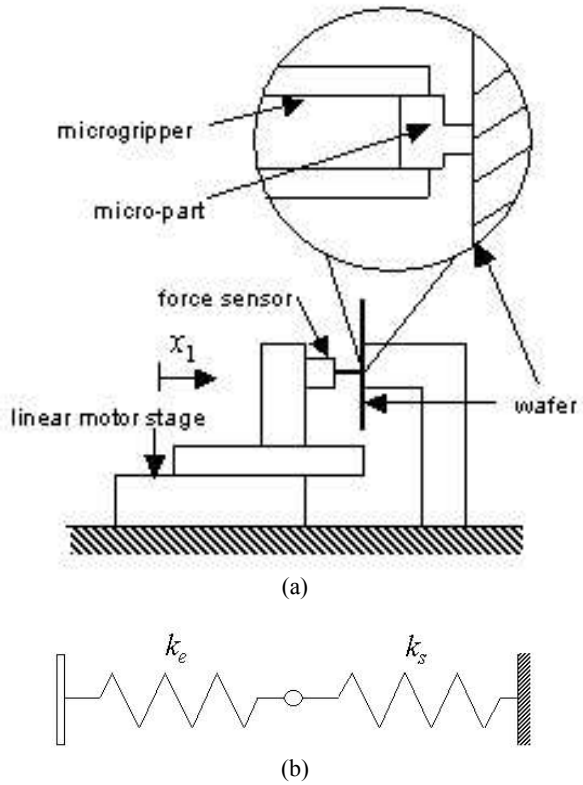

Fig. 5 Contact between microassembly robot and process wafer. a) system schematic b) contact stiffness model

k_e and k_s are dependent on the particular microassembly operation. Furthermore, this contact model will not be used in the control design. Instead it is assumed that the contact force, measured by the force sensor, will be fed back to the controller, as in typical direct force control applications.

MICROASSEMBLY FORCE CONTROL

In this paper, the objective for designing a force controller for microassembly is to be able achieve a desired contact force without *a priori* knowledge of the stiffness of the contact surface. In addition, force tracking will be required during some operations. The two accepted approaches for designing a dynamic force controller are impedance control and direct force control. Both approaches are generally applicable to microassembly, and both will eventually find application in this field. However, impedance control requires a stiffness value for the contact surface and typically does not achieve satisfactory force tracking results. Due to these drawbacks, direct force control has been chosen for the presented research. It should be noted that both approaches require an inner motion loop. Therefore, the robust motion controller discussed in following subsection is applicable to both approaches.

The approach to designing a direct force control loop for a linear motor stage is similar to that used in standard robotics. However, there are several distinct differences which should be noted. Most importantly, the regulated force will be in the range of millinewtons to micronewtons. Therefore, high precision positioning is required to regulate such minute forces. This will necessitate direct compensation for the friction and force ripple effects described in the previous section, which are highly nonlinear. A robust motion controller which utilizes a friction observer will be used to achieve the required positioning accuracy, which is discussed in following subsection. The force control will then be developed based on this motion control approach.

Robust Motion Control Design

Before designing the robust motion controller, the dynamic system shown in Eqs. (2-3) must be placed into a tracking error form using the coordinate transformations $\tilde{x}_1 = x_1 - x_{1d}$ and $\tilde{x}_2 = x_2 - \dot{x}_{1d}$ such that:

$$\dot{\tilde{x}}_1 = \tilde{x}_2 \tag{10}$$

$$\dot{\tilde{x}}_2 = -\frac{1}{m}\left(f_f + f_r\right) - \ddot{x}_{1d} + \frac{K_f}{m}u \tag{11}$$

where x_{1d} is the desired position trajectory. The control design used in this paper is sliding mode control, which has been discussed extensively in the literature (see [17]). It has been chosen due to its robustness properties, straightforward design approach and applicability to nonlinear systems. The first step in the design process is to define a sliding surface. In this case, a first order surface is chosen as follows:

$$s = \tilde{x}_2 + \lambda \tilde{x}_1 \tag{12}$$

where λ is a positive valued design parameter. Based on the requirement that the control input, u, must be designed to force the system to the sliding surface, the control law is chosen as:

$$u = -\frac{m}{K_f}\left(-\frac{1}{m}\left(\hat{f}_f + \hat{f}_r\right) - \ddot{x}_{1d} + \lambda \tilde{x} + \phi s + \frac{\rho s}{\left(s^2 + \varepsilon^2\right)^{1/2}} \right) \tag{13}$$

where $\hat{f}_f$ and $\hat{f}_r$ are the nominal values of the friction force and force ripple, respectively, ϕ and ε are positive valued design parameters, and ρ is the switching gain. The final term in Eq. (13) is a continuous approximation for the sliding modes switching law, which is referred to as a smooth norm switching law. Substituting Eq. (13) into Eqs. (10-11) results in the following closed loop system:

$$\dot{\tilde{x}}_1 = \tilde{x}_2 \tag{14}$$

$$\dot{\tilde{x}}_2 = -\phi\lambda x_1 - (\phi + \lambda)x_2 - \frac{1}{m}\left(\left(f_f - \hat{f}_f\right) + \left(f_r - \hat{f}_r\right)\right) - \frac{\rho s}{\left(s^2 + \varepsilon^2\right)^{1/2}} \tag{15}$$

An appropriate choice of the switching gain, ρ, which guarantees stability of the closed loop system, with uncertainty in the friction and force ripple functions, f_f and f_r, can be

determined using Lyapunov stability based on the following Lyapunov function:

$$V = \frac{1}{2}s^2 \tag{16}$$

Taking the time derivative of Eq. (16) and utilizing Eqs. (12, 14-15), results in the following expression:

$$\dot{V} = -\phi s^2 - s\left(\frac{\rho s}{\left(s^2+\varepsilon^2\right)^{1/2}} + \frac{1}{m}\left(\left(f_f - \hat{f}_f\right) + \left(f_r - \hat{f}_r\right)\right)\right) \tag{17}$$

Therefore, given the proper choice of the switching gain, ρ, Eq. (17) can be rendered negative definite for some region of attraction for the sliding surface, *s*. The design of the switching gain will be based on the representation of the functions $\hat{f}_f$ and $\hat{f}_r$.

The estimated friction force used in the controller is provided by a friction observer based on the concept discussed by Canudas de Wit et al. [11]. The friction observer is defined as follows:

$$\dot{\hat{z}} = x_2 - \frac{|x_2|}{\hat{g}(x_2)}\hat{z} - k\left(x_1 - x_{1d}\right) \tag{18}$$

where:

$$\hat{g}(x_2) = \frac{1}{\hat{\sigma}_0}\left(\hat{F}_c + \left(\hat{F}_s - \hat{F}_c\right)e^{-\left(x_2/x_{2s}\right)^2}\right) \tag{19}$$

and the resulting nominal friction force is :

$$\hat{f}_f = \hat{\sigma}_0 z + \hat{\sigma}_1 \dot{z} + \hat{\sigma}_2 x_2 \tag{20}$$

All of the parameters with a (^) are nominal or average values. The parameter *k* is a gain which is used to tune the convergence of the friction observer. Therefore, this model includes the uncertainty between the actual parameter values and those used in the control design, unlike the approach in [11]. However, this uncertainty will not be addressed directly, parameter by parameter. Instead upper bounds on the friction force will be used in the sliding mode switching gain.

Based on the steady state friction force shown in Eq. (7), it can be shown that:

$$\left|f_f - \hat{f}_f\right| \le F_s + \left(\sigma_{2\max} - \hat{\sigma}_2\right)|x_2| \tag{21}$$

where $\sigma_{2\max}$ is the maximum possible viscous friction coefficient. Furthermore, the nominal force ripple can be written as:

$$\hat{f}_r = \hat{A}_{r1}\sin\hat{\omega}x_1 + \hat{A}_{r2}\cos\hat{\omega}x_1 \tag{22}$$

Therefore, the maximum difference between the actual ripple force and the nominal model can be written as:

$$\left|f_r - \hat{f}_r\right| \le 2A_{r1\max} + 2A_{r2\max} \tag{23}$$

Based on Eqs. (21) and (23), Eq. (17) can be reduced to :

$$\dot{V} \le -|s|\left(\frac{\rho|s|}{\left(s^2+\varepsilon^2\right)^{1/2}} - \Delta\right) \tag{24}$$

where:

$$\Delta = \frac{1}{m}\left(F_s + \left(\sigma_{2\max} - \hat{\sigma}_2\right)x_2 + 2A_{r1\max} + 2A_{r2\max}\right) \tag{25}$$

Choosing the sliding mode switching gain such that $\rho = \eta\Delta$ results in the following bounds on the steady state error for reaching the sliding surface:

$$|s| \le \frac{\varepsilon}{\left(\eta^2 - 1\right)^{1/2}} \tag{26}$$

It can then be determined that the tracking error is bounded such that:

$$|x_1| \le \frac{\varepsilon}{\lambda\left(\eta^2 - 1\right)^{1/2}} \tag{27}$$

Therefore, the tracking error is solely dependent on the design parameters, λ, η, and ε. However, as the tracking error bounds are reduced by either increasing η or decreasing ε, the chance of chattering in the control signal increases, which would be unacceptable when the microassembly robot is in contact with an object. The tracking error and control effort must therefore be considered equally when choosing the parameters. The force control design based on this motion control approach will now be discussed.

Force Control Design

The general approach to direct force control, as discussed by Siciliano and Villani [18], uses an inner motion loop which is fed a position command from an outer force control loop. The closed loop system is fed a desired force signal which is compared to the measured force at the robot end-effector. The error between the desired and actual force is then used to generate a position command based on the force control law. This approach has been adopted for the microassembly force control, where the robust motion controller discussed in the previous section will be used as the inner motion loop. However, in addition to the outer force control loop, a high-gain trajectory estimator is included so that the inner motion control receives complete trajectory information. This is expected to improve the performance of the force regulation by using tracking control as opposed to set point control. A block diagram of the proposed closed loop system is shown in Fig. 6.

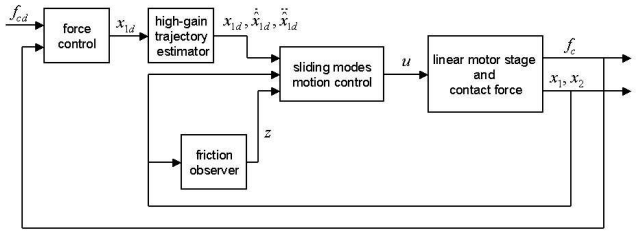

Fig. 6 Force control with inner robust motion control loop and trajectory estimator

The force control law which has been chosen is a proportional-integral equation. This controller, which is typical for direct force control, generates the position trajectory x_{1d}, based on the force regulation error. The control law can be written as :

$$x_{1d} = \frac{1}{\phi \lambda}\left(K_p \tilde{f}_c + K_i \int_0^t \tilde{f}_c \, d\xi \right) \tag{28}$$

where K_p and K_i are the proportional and integral gains, respectively. The force regulation error, $\tilde{f}_c$, is defined as $\tilde{f}_c = f_{cd} - f_c$ where f_{cd} is the desired contact force. The motion control gains, ϕ and λ, are included in Eq. (28) so that the gain selection for the motion and force loops are decoupled, as suggested by Siciliano and Villani [18].

The force control law in Eq. (28) only generates a position trajectory. However, the robust motion controller is designed to use a full-state trajectory to provide robust tracking. Therefore, a method for estimating the first and second derivatives of the position trajectory is required . A high-gain observer, such as discussed by Esfandiari and Khalil [19], will be used for this purpose. The high-gain trajectory estimator is defined as:

$$\begin{bmatrix} \dot{y}_1 \\ \dot{y}_2 \\ \dot{y}_3 \end{bmatrix} = \begin{bmatrix} -\beta_1/\tau & 1 & 0 \\ -\beta_2/\tau^2 & 0 & 1 \\ -\beta_3/\tau^3 & 0 & 0 \end{bmatrix} \begin{bmatrix} y_1 \\ y_2 \\ y_3 \end{bmatrix} + \begin{bmatrix} \beta_1/\tau \\ \beta_2/\tau^2 \\ \beta_3/\tau^3 \end{bmatrix} x_{1d} \tag{29}$$

where $y_1 = \hat{x}_{1d}$, $y_2 = \dot{\hat{x}}_{1d}$, and $y_3 = \ddot{\hat{x}}_{1d}$, and β_1, β_1, β_1, and τ are design gains which determine the performance of the observer. The bandwidth of the observer should be designed to be higher than that of the robust motion controller. This will guarantee that the trajectory estimates do not limit the motion response of the closed loop system. The estimator is referred to as a high-gain observer because as $\tau \to 0$, the gain approaches infinity and the estimates become exact. The motion controller will use the actual position trajectory from the force control law in Eq. (28), and the two trajectory estimates $\dot{\hat{x}}_{1d}$, and $\ddot{\hat{x}}_{1d}$. The results of simulation tests using the proposed controller will now be discussed.

SIMULATION RESULTS

The force control approach discussed in the previous section has been tested on the proposed dynamic model in simulation. The model parameters used in these simulations are the same as those parameters used in the presented open loop simulations. In addition, the control parameters which were used are ϕ = 128.3, λ = 311.7, ε = 0.2, η = 1.4, k = 5, K_p = 2000, and K_i = 5000. The contact stiffness parameters were assumed to be $k_e = 10^5$ N/m and $k_s = 10^7$ N/m. The stiffness values were chosen based on the fact that micro-parts are typically made of materials with a high Young's modulus and dimensional scaling indicates that they would in general be very stiff. The difficulty in dealing with high stiffness parts could be addressed by designing a microgripper with a low stiffness for passive compliance. This approach was not considered in the presented simulation results.

The objective of these simulations was to study how the controller performs when there is uncertainty in the friction and force ripple parameters. In the first set of tests, the performance in the presliding regime, or micro-dynamics region, was examined. The initial position of the linear motor stage was set at a distance of 5 μm from the process wafer. The desired contact force was set at 50 μN. In the first round of this test, the actual friction and ripple force parameters were set to be 5 % greater than the nominal values. The results of this test are shown in Fig. 7. The linear motor stage successfully reaches the wafer and the desired contact force is achieved. The only undesirable feature of the stage performance is the spike in the measured force during initial contact. A close-up of this spike is shown in Fig. 8. Several intermittent contacts are made due to the high stiffness of the part and surface. However, the oscillation is quickly suppressed and the desired force is obtained. The magnitude of this spike is largely dependent on the force control gains and must be tuned properly to avoid overloading of the microgripper, force sensor and micro-parts. Similar results have also been observed when the actual friction and force ripple parameters are 5 % smaller than the nominal values.

A second set of tests examined the performance of the controller when the stage is in the sliding regime. The initial distance between the stage and wafer was set at 100 μm. This initial distance guarantees that the stage transitions to the sliding regime before contact, based on preliminary tests for finding the breakaway point. The results of this test when the actual friction and force ripple parameters are 5 % greater than the nominal values are shown in Fig.9. These results are very similar to those gained when the system is in the presliding regime. Similar results were also found when the parameters were set to be 5 % less than the nominal values. The main difference between the two sets of tests was in the time it took for the linear motor stage to reach the wafer. These results verify the effectiveness of the proposed control approach based on the derived model.

DISCUSSION

The presented research has concentrated on developing a force control approach for linear motor stages, in which the friction and force ripple characteristics were considered to be the dominant forces. Based on this assumption, it has been

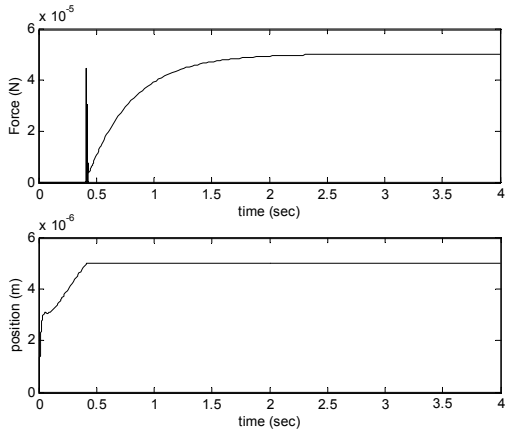

Fig. 7 Force and position results when the linear motor stage is initially 5 μm away from the wafer

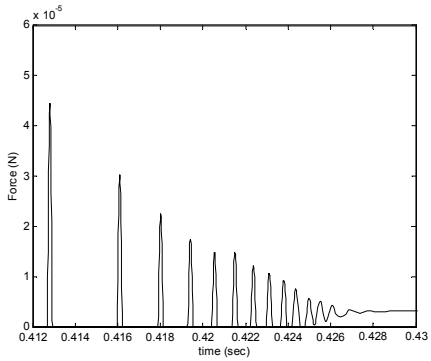

Fig. 8 Close-up of force chatter during initial contact

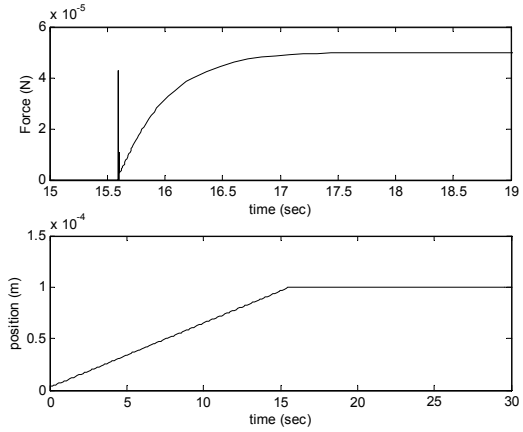

Fig. 9 Force and position results when the linear motor stage is initially 100 μm away from the wafer

shown through simulation results that the proposed control design is effective at controlling the contact force, even when there is uncertainty in the friction and force ripple parameters on the order of ± 5 %. However, there are many other factors which will influence the success of the force controller that have not been considered. Some of these factors will now be discussed briefly as motivation for the further development of microassembly capabilities.

One significant factor which was not considered in the control design is the resolution, or quantization, of the feedback for the linear motor stage position. The typical feedback sensor found in linear motor stages is a linear encoder. The best possible resolution obtainable with these sensors in most commercially available mechanisms is on the order of 20 nm. This is significant because the operation of the inner motion loop is dependent on the position feedback. Switching between two discrete values on the encoder could cause oscillations on order of 20 nm during a microassembly operation. Whether this will have an effect on the success of the operation will be dependent on the respective stiffnesses of the microgripper, micro-component and process wafer.

In addition, the resolution of the force sensor will also determine the smoothness of the contact force. However, most force sensors are based on analog electronics. Therefore, the quantization is not an issue, but the sensor noise must be examined. The magnitude of the sensor noise should be several orders of magnitude below the desired lower bound on the measured force. This is difficult to achieve when using existing sensor technology. Although sensitive force sensors with resolution on the order of nanonewtons are available, such as the piezo cantilevers used in atomic force microscopes, these devices are not easily integrated into a microgripper. Therefore, more research on the development of micro force sensors is required, especially multi-axis devices.

Uncertainties in the linear motor stage motion and geometry will also add to these difficulties. Off-axis errors in the motion of the stage result from misalignment of the bearings and machining tolerances. These errors can be on the order of several micrometers for commercially available mechanisms. Thermal effects also change the geometry of the stage, adding to these errors. However, it is believed that the sum of these errors will have less effect on the force control than on the motion control. This is due to the fact that the force controller is only dependent on the relative motion between the linear motor stage and work piece. Regardless, an approach to compensating for these errors is required for successful microassembly operations.

A final important factor is the presence of adhesion forces, such as electrostatic, capillary and van der Waals forces. These forces play an important role in the motion of a micro-component, and can have positive or negative effects on the microassembly operations. It is unclear how these forces will interact with the force controller. However, Nelson et al. [9] have noted the presence of adhesion forces while performing force control at the nanonewton level. Therefore, they should be considered when designing a force controller for microassembly. In particular, the possibility of these forces destabilizing the closed loop system should be examined.

These four topics highlight the intricacies of developing a functional microassembly robot with force control capabilities. The impact which these factors have on microassembly operations will have to be determined experimentally, which will be the subject of future research.

CONCLUSION

This paper has addressed the problem of designing a force control law for linear motor stages which would enable force regulation on the order of micronewtons. This objective is set

by the need for high-speed, high-precision, microassembly robots which can manipulate micro-parts for the assembly of hybrid MEMS. The modeling of a linear motor stage has concentrated on capturing the dominant forces which hinder high-precision motion control, which are friction and force ripple. The derived dynamic equations incorporate a dynamic friction model which has previously been shown to be very effective at representing the presliding and sliding regimes inherent in friction contacts. Based on this dynamic model, a robust inner motion control loop and a force control law have been designed for force regulation. This controller has been tested in simulation, and the system has been shown to regulate the desired force even when the friction and force ripple parameters vary on the order of ± 5 %.

In future research, this approach will be implemented experimentally on a microassembly robot which is currently being developed. The results of this paper will be useful for determining the robot's level of dexterity for manipulating micro-parts. Furthermore, the results will be used to determine how these micro-parts will be affected by chattering during initial contact. Several extensions of the presented approach will also be investigated, including force tracking, hybrid force/position control for microassembly, and friction parameter identification. Furthermore, several factors which will play a role in the success of microassembly have been discussed, including sensor resolution, sensor noise, off-axis errors, thermal effects and adhesion forces. These topics will also be explored with respect to the presented research.

ACKNOWLEDGMENTS

This research was performed while the first author held a National Research Council Postdoctoral Research Associateship Award at the National Institute of Standards and Technology.

REFERENCES

[1] Madou, M. J., 2001, *Fundamentals of Microfabrication*, CRC Press, Boca Raton, FL.

[2] Cohn, M. B., Bohringer, K. F., Noworolski, J. M., Singh, A., Keller, C. G., Goldberg, K. Y., & Howe, R. T., 1998, "Microassembly technologies for MEMS", *Proceedings of the SPIE Conference on Microfluidic Devices and Systems*, Santa Clara, CA, pp. 2-16.

[3] Bohringer, K. F., Fearing, R. S., & Goldberg, K. Y., 1999, "Microassembly", *Handbook of Industrial Robotics*, John Wiley & Sons, New York.

[4] Van Brussel, H., Peirs, J., Reynaerts, D., Delchambre, A., Reinhart, G., Roth, N., Weck, M., & Zussman, E., 2000, "Assembly of microsystems", *Annals of the CIRP*, pp. 451-472.

[5] Xu, L. & Yao, B., 2001, "Adaptive robust precision motion control of linear motors with negligible electrical dynamics: theory and experiments", *IEEE Transactions on Mechatronics*, **6**, pp. 444-452.

[6] Tan, K. K., Huang, S. N., & Lee, T. H., 2002, "Robust adaptive numerical compensation for friction and force ripple in permanent-magnet linear motors", *IEEE Transactions on Magnetics*, **38**, pp. 221-227.

[7] Wu, S. H. & Perng, M. H., 2001, "A switching controller for fast nano-positioning control", *Proceedings of the IEEE Conference on Nanotechnology*, pp. 168-173.

[8] Ro, P., Wonbo, S., & Jeong, S., 2000, "Robust friction compensation for submicrometer positioning and tracking for a ball-screw-driven slide system", *Precision Engineering*, **24**, pp. 160-173.

[9] Nelson, B. J., Zhou, Y., & Vikramaditya, B., 1998, "Sensor-based microassembly of hybrid MEMS devices", *IEEE Control Systems Magazine*, **18**, pp. 35-45.

[10] Tanikawa, T., Kawai, M., Koyachi, N., Arai, T., Ide, T., Kaneko, S., Ohta, R., & Hirose, T., 2001, "Force control system for autonomous micro manipulation", *Proceedings of the IEEE International Conference on Robotics and Automation*, Seoul, Korea, pp. 610-615.

[11] Canudas de Wit, C., Olsson, H., Astrom, K. J., & Lischinsky, P., 1995, "A new model for control of systems with friction", *IEEE Transactions on Automatic Control*, **40**, pp. 419-425.

[12] Shimada, E., Thompson, J. A., Yan, J., Wood, R., & Fearing, R. S., 2000, "Prototyping millirobots using dextrous microassembly and folding", *Proceedings of the ASME IMECE/DSCD*, Orlando, FL, pp. 933-940.

[13] Zhou, Q., Aurelian, A., del Corral, C., Esteban, P. J., Kallio, P., Chang, B., & Koivo, H. N., 2001, "A microassembly station with controlled environment", *SPIE Conference on Microrobotics and Microassembly*, Boston, MA, pp. 252-260.

[14] Yang, G., Gaines, J. A., & Nelson, B. J., 2001, "A flexible experimental workcell for efficient and reliable wafer-level 3D microassembly", *Proceedings of the IEEE International Conference on Robotics and Automation*, Seoul, Korea, pp. 133-138.

[15] Kwon, S., Chung, W. K., & Youm, Y., 2001, "On the coarse/fine dual-stage manipulators with robust perturbation compensator", *Proceedings of the IEEE International Conference on Robotics and Automation*, Seoul, Korea, pp. 121-126.

[16] Dechev, N., Cleghorn, W. L., & Mills, J. K., 2002, "Micro-assembly of microelectromechanical components into 3-D MEMS", *Canadian Journal of Electrical and Computer Engineering*, **27**, pp. 7-15.

[17] Edwards, C. & Spurgeon, S. K., 1998, *Sliding Mode Control: Theory and Applications*, Taylor & Francis, London.

[18] Siciliano, Bruno & Villani, Bruno, 1999, *Robot Force Control*, Kluwer, Boston.

[19] Esfandiari, F. & Khalil, H. K., 1992, "Output feedback stabilization of fully linearizable systems", *International Journal of Control*, **56**, pp. 1007-1037.